Coordination motifs and large-scale structural organization in atomic clusters

Zhu Yang and Lei-Han Tang
Department of Physics, Hong Kong Baptist University, Kowloon Tong, Hong Kong SAR, China

(Received 2 October 2008; revised manuscript received 23 November 2008; published 6 January 2009; corrected 12 January 2009)

The structure of nanoclusters is complex to describe due to their noncrystallinity, even though bonding and packing constraints limit the local atomic arrangements to only a few types. A computational scheme is presented to extract coordination motifs from sample atomic configurations. The method is based on a clustering analysis of multipole moments for atoms in the first coordination shell. Its power to capture large-scale structural properties is demonstrated by scanning through the ground state of the Lennard-Jones and C_{60} clusters collected at the Cambridge cluster database.

DOI: 10.1103/PhysRevB.79.045402 PACS number(s): 61.46.−w, 36.40.Mr, 61.43.−j, 64.70.Nd

I. INTRODUCTION

Nanoscale atomic clusters have attracted a great deal of attention in recent years due to their promising applications in catalysis, photonics, and bioimaging.[1–3] The functionality of these clusters is controlled by their structure, which may assume a variety of forms as a result of the generally complex energy landscape governing the low-energy cluster conformations.[4] Atomic arrangements in these clusters generally do not follow the crystal structure of the corresponding bulk material but may nevertheless possess certain regularities. Suitable representation of these structures, particularly for small- and medium-sized clusters, is important for uncovering mechanisms that underlay their thermodynamic stability and functionality.

Traditionally, atomic clusters of high point symmetry are described in terms of the five Platonic solids and their truncated polyhedra.[4,5] Starting from, say, a 13-atom core as illustrated in Fig. 1, successive layers of atoms can be added to produce clusters of "magic size" which feature prominently in spectroscopic measurements. Two particularly well-known series are the Mackay icosahedra (MIC) (Ref. 6) that grow from Fig. 1(c) and the Marks decahedra (MD) (Ref. 7) that grow from Fig. 1(d). Noble-gas nanoclusters follow the Mackay icosahedra series up to a few thousand atoms before switching to the Marks decahedra series.[8] Both types of clusters can be viewed as multiply twinned particles that take advantage of the low-energy surfaces of the constituting face-centered-cubic (fcc) grains. At even larger sizes, accumulation of strain in the particle drives a transition to the single crystal structure, although the size at which such transition takes place is still debated.[9]

Real structures often contain defects and imperfections as compared to the ideal ones.[10] Recently, Polak and Patrykiejew[11,12] investigated medium-sized Lennard-Jones (LJ) clusters of a few hundred atoms obtained in Monte Carlo simulations at low temperatures. They proposed a scheme to describe the interior structure of an atomic cluster in terms of the four "coordination polyhedra" of Fig. 1. Indeed, when atoms with a particular type of coordination are displayed, large-scale features such as cubic domains or polyicosahedral grains become readily visible. Polak applied the scheme to describe the structure evolution during cooling runs and in cluster growth starting from a seed crystallite. It is conceivable that insights generated from such studies can assist experimental designs aimed at producing a particular class of nanoclusters.

The four coordination polyhedra in Fig. 1 were identified by Polak through visual inspection of a large number of atomic configurations. Here we extend Polak's work to construct a systematic and robust computational methodology for local coordination analysis and large-scale structure identification. This is necessary as the local atomic structures often contain distortions or even belong to unknown categories. The idea is quite simple. Given a set of atomic coordinates, we first compute the radial distribution function to determine a suitable cutoff distance for the first coordination shell. We then parametrize the coordination shell configuration of each interior atom using the multipole moments Q_l of the shell atoms.[13] The data set is examined for their clustering properties in the "shape space" spanned by the Q_l's. Each well-defined cluster in the shape space represents a reoccurring local structural unit which we call a "coordination motif." Atoms in the same cluster are then assigned the same "type." The scheme allows for fast classification of interior atoms and their local neighborhoods. The geometric shape of individual motifs and their spatial organization provide valuable information on large-scale structure organization. The MIC and the MD series, for example, each possesses a unique composition profile of the coordination motifs. In such cases, the motif content alone can be used for accurate structure association.

The paper is organized as follows. In Sec. II we describe the computational procedure for the identification of structure motifs. The ground-state LJ clusters are used as examples. Section III contains a discussion of large-scale structure organization based on the spatial distribution of motifs

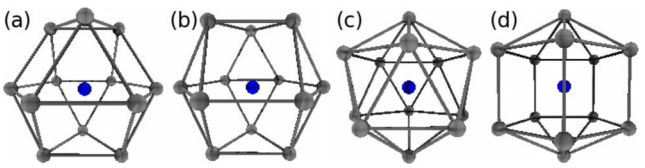

FIG. 1. (Color online) The first coordination shell at coordination number of 12. (a) face-centered cubic (fcc), (b) hexagonal-close-packed (hcp) structure, (c) icosahedral (ico), and (d) decahedral (dec).

 ©2009 The American Physical Society

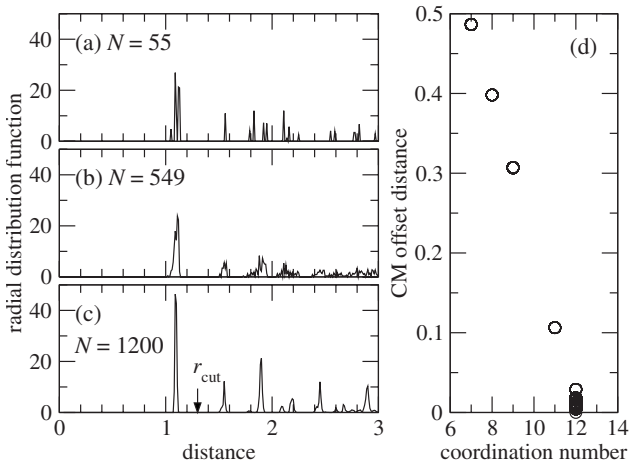

FIG. 2. (a)–(c) Radial distribution function of LJ clusters at three selected sizes. (d) The distance between the CM of the first coordination shell and the center atom against the coordination number for all atoms in a $N=549$ cluster. Here $r_{cut}=1.3$.

of different types. Particular emphasis is given to the decagonal motifs that define local pentagonal symmetry axis for twinning. Section IV contains a summary of our findings and conclusions from the work.

II. LOCAL STRUCTURE MOTIF IDENTIFICATION

The procedure for the coordination motif identification consists of three steps: (i) specification of the first coordination shell through an analysis of the radial distribution function, (ii) parametrization of the atomic configuration for completed shells, and (iii) clustering of the data to determine the most frequently occurring coordination motifs. We illustrate the method in the description of the (putative) ground state of LJ clusters with up to $N=1610$ atoms available at the Cambridge cluster database (CCD).[14,15] Figures 2(a)–2(c) show the radial distribution function obtained from the histogram of pairwise distances $r_{ij}=|\mathbf{r}_i-\mathbf{r}_j|$ for three selected atomic clusters at $N=55$, 549 (complete Mackay icosahedra), and 1200 at a bin size $\Delta r=0.01$ (in units of the LJ radius σ). Note that the minimum of the LJ potential is at $r_{min}=2^{1/6}\sigma \simeq 1.12\sigma$. In all three cases, there are well-defined distance gaps which allow for unambiguous identification of first and second coordination shells for all atoms on the cluster. The position of the first two peaks are at $r_1 \simeq 1.1$ and $r_2 \simeq 1.55$, respectively, with the ratio $r_2/r_1 \simeq 1.4$ which corresponds well to the value $\sqrt{2}$ for the fcc or hcp structure. The plot suggests a cutoff distance $r_{cut}=1.3$ for atoms to be included in the first coordination shell. To distinguish interior from surface atoms, we compute the offset distance r_{offset} between the center atom and the center of mass (CM) of its first coordination shell. Figure 2(d) shows a scatter plot of r_{offset} against the coordination number for all atoms on the $N=549$ cluster. The approximately linear behavior of the data indicates that completed shells have 12 atoms.

The 12-atom neighborhoods as shown in Fig. 1 are distinguished from one another by the angular distribution of atoms on the shell. Provided the distance of shell atoms to the center atom falls in a narrow range, the shell configuration is well represented by a density function $\rho(\theta,\phi)=\Sigma_k \delta(\theta-\theta_k,\phi-\phi_k)$ on the unit sphere, where (θ_k,ϕ_k) are the polar coordinates of shell atom k with the origin on the center atom. Consider now the "multipole" expansion in the spherical harmonics,

$$\rho(\theta,\phi)=\sum_{l,m} a_{lm} Y_{lm}(\theta,\phi), \tag{1}$$

where $a_{lm}=\Sigma_k Y^*_{lm}(\theta_k,\phi_k)$. The multipole moments of the shell configuration are given by[13]

$$Q_l \equiv \frac{1}{C}\sqrt{\frac{4\pi}{2l+1}\sum_{m=-l}^{l}|a_{lm}|^2}=\sqrt{\frac{4\pi}{2l+1}\sum_{m=-l}^{l}|\bar{Y}^*_{lm}|^2}, \tag{2}$$

where C is the number of shell atoms and the overline bar denotes average over the shell. Note that $Q_l=1$ (all l) if there is only one atom on the shell. It is easy to verify that the multipole moments Q_l are invariant with respect to a rigid rotation of the shell density.

In Ref. 11, the moments Q_4 and Q_6 are used to distinguish the four atomic configurations shown in Fig. 1. We propose here a more general approach based on the clustering property of interior atoms in the shape space spanned by the multipole moments $\{Q_l\}$. Atoms that are close to each other in this representation have very similar neighborhoods. Strong clustering of the data points in the shape space suggests existence of only a few coordination motifs. Standard clustering methods[16] can then be used to assign coordination motifs to the atoms. On the other hand, weak clustering would imply a more continuous spectrum of local neighborhoods without a clear local structural preference.

Figure 3 shows the multipole moments Q_4, Q_6, and Q_8 for all interior atoms on the ground-state LJ clusters at the three selected sizes. In all cases, the data exhibit very strong clustering which agrees well to the four shell configurations in Fig. 1. Note that the cluster that corresponds to the decagonal motif has a slightly bigger spread than the other three clusters. Inspection of the atomic coordinates show that the decahedron has a shorter axis in the two smaller systems and is elongated slightly in the $N=1200$ case. The moment Q_8 per-

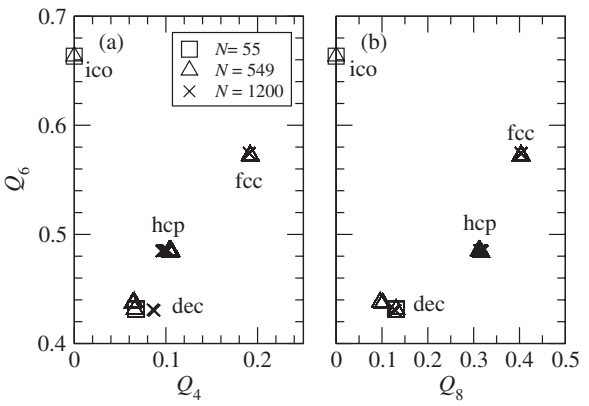

FIG. 3. Scatter plot of the multipole moments of interior atoms on the ground-state LJ clusters at three different cluster sizes. (a) Q_6 versus Q_4 and (b) Q_6 versus Q_8.

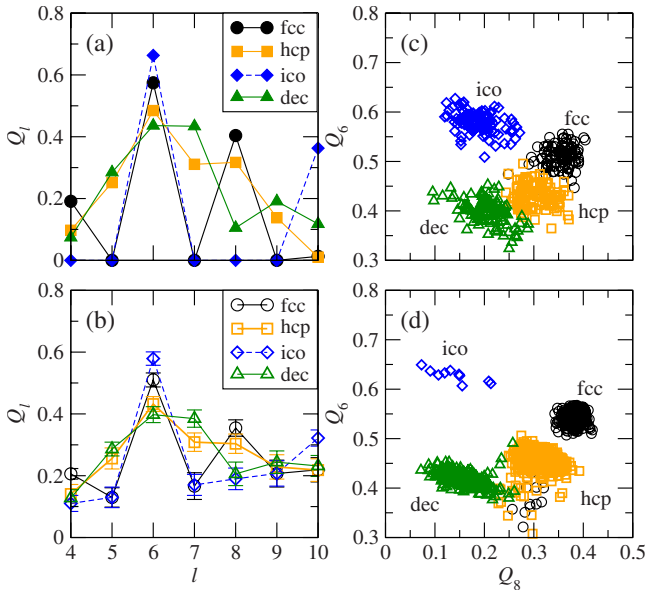

FIG. 4. (Color online) The multipole moments Q_l for regular (solid symbols) and noisy (open symbols) polyhedra. (a) Q_l against l for the four regular polyhedra and (b) averaged Q_l against l for randomized shell configurations at a noise strength $\Delta\theta=0.07\pi$. Error bars are obtained from the standard deviation over 100 random samples. (c) Q_6 versus Q_8 for individual shell configurations at $\Delta\theta=0.07\pi$. The symbols are chosen in each case to correspond to the shell configuration before randomization. (d) Q_6 versus Q_8 from ten randomized samples of the $N=549$ LJ cluster at $\Delta r=0.1r_{\min}$ (see text).

forms better than Q_4 in discriminating the hcp and dec motifs.

Thermal fluctuations lead to distortions of the polyhedra so that the corresponding data points in the shape space are more spread out than in the ground state. We have investigated the dependence of the width of such clouds on the noise strength using simulated data. Starting from each of the four regular polyhedra, we randomly displace the 12 shell atoms laterally to create noisy density patterns. The displacement of each atom is restricted to within a distance $\Delta r=R\Delta\theta$ from its original position, where R is the radius of the coordination shell and $\Delta\theta$ defines the noise strength. Figures 4(a)–4(c) show a comparison of the Q_l's for the ideal (solid symbols) and noisy (open symbols) structures at $\Delta\theta=0.07\pi$. In the latter case, 100 shell configurations are generated from each of the four regular polyhedra. Error bars on the data in Fig. 4(b) represent standard deviations over the 100 samples. From Fig. 4(c) it is seen that the icosahedral coordination motif is well separated from the other three and can be easily recognized. The hcp motif is sandwiched between the fcc and dec motifs in the shape space and is more easily deformable into either of the two. At $\Delta\theta=0.07\pi$, the hcp cluster already begin to merge with the fcc and dec clusters. The data (with error bars) in Fig. 4(b) suggest that either Q_6 or Q_7 can be used to separate the hcp from the fcc motif, while Q_8 can be used to separate the hcp from the dec motif. Enhanced performance is expected when the classification is done in the high-dimensional shape space which combines information from all the Q_l's.

We have also generated noisy atomic clusters by adding random displacements to the ground-state LJ configurations. Each component of the atomic displacement is taken to be Gaussian distributed with zero mean and a standard deviation h. The resulting atomic clusters are analyzed following the general procedure described above. Figure 4(d) shows an example of the local coordination data obtained from ten randomized samples of the $N=549$ cluster at $h=0.06r_{\min}$ or $\Delta r=3^{1/2}h=0.1r_{\min}$. Only atoms with coordination number of 12 are included. The symbols used for the selected atoms in the plot correspond to their coordination type in the ground-state cluster. It is seen that the data at this noise level still form well-defined clusters in the shape space, with the majority of atoms keeping their original identity. There are however a few outliers (points with Q_6 less than 0.35) where the shell configuration has changed so significantly that they can no longer be classified into any of the four categories. Closer inspection of the atomic configurations indicates that such cases are usually accompanied by large displacements of atoms in the neighborhood, so that a more careful definition of the first coordination shell for the atom in question is needed. Interestingly, the Lindemann criterion for crystal melting sets a limit on Δr to be around (10–12)% of the nearest-neighbor distance at the bulk melting point.[17] From our simulation studies, this is also the noise level around which different coordination motifs start to become indistinguishable from each other.

III. COMPOSITION PROFILE AND LARGE-SCALE STRUCTURE ORGANIZATION OF ATOMIC CLUSTERS

Using the moment pair (Q_6,Q_8) as classifier, we computed the composition profile $c_\alpha=N_\alpha/N_{\text{interior}}$ of the four coordination motifs for all ground-state LJ clusters in the size range $N=13-1610$. Here N_α is the number of $\alpha=\text{fcc},\text{hcp},\text{ico},\text{dec}$ atoms in the cluster interior and N_{interior} is the total number of interior atoms. Results are shown in Fig. 5. Each curve gives the percentage of a particular motif in the atomic cluster against the cluster size. As a reference, Table I lists the number of interior atoms of each type for complete Mackay icosahedra and Marks decahedra as a function of the layer number n. Also given is the total number of interior atoms N_{interior} as well as the cluster size N. Using these expressions, we computed the concentration of the fcc motif for the MIC and the MD series, as indicated by the dashed and dashed-dotted lines in Fig. 5(a), respectively. The overall trend of structure evolution is evident. Beyond $N=147$ (three completed shells in an icosahedral structure), the ground state essentially alternates between these two structures. The main transition between the Mackay icosahedra-dominated regimes at smaller sizes to the Marks decahedra-dominated regime at larger sizes takes place at around $N=1030$, indicated by an upward jump in the c_{fcc} curve in Fig. 5(a). Windows exist on either side of the transition where the minority series pops in. The physical mechanism behind these transitions, which has something to do with the competition between strain and surface energies, has already been discussed extensively in the literature.[18]

We have examined the spatial distribution of the coordination motifs on large atomic clusters. Figure 6 shows two

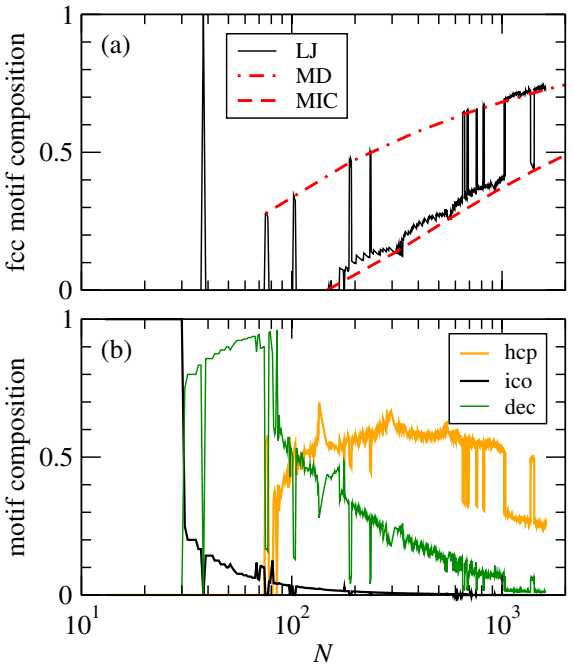

FIG. 5. (Color online) Composition profile of (a) the fcc motif and (b) hcp, ico, and dec motifs in the ground-state LJ clusters. Dashed and dashed-dotted lines in (a) give the theoretical values of c_{fcc} for complete Mackay icosahedra and Marks decahedra, respectively.

such examples taken from the ground-state LJ clusters at (a) $N=923$ (MIC) and (b) 1103 (MD). Only interior atoms at the center of the following three types of polyhedra are plotted: blue (black) for icosahedron, green (light gray) for decahedron, and orange (dark gray) for hcp. The icosahedrally coordinated atom is only present at the center of the MIC cluster in Fig. 6(a). The decagonally coordinated atoms are located on the fivefold symmetry axes in both clusters, while the hcp atoms form two-dimensional sheets that separate the fcc grains (not shown) at symmetry-related crystallographic orientations.

Clusters of size less than three atomic layers exhibit a greater variety of organizational behavior due to the more subtle and delicate balance of packing, strain, and surface effects. Figure 7 shows the composition profiles in this size range for two representative classes of ground states in the CCD: the LJ clusters (solid symbols) discussed above and

TABLE I. Number of ico, dec, hcp, and fcc-coordinated atoms in the complete MIC and MD series. The total number of completed shells (including surface atoms) is given by n.

	MIC	MD
N_{ico}	1	0
N_{dec}	$12(n-1)$	$2n-1$
N_{hcp}	$15(n-1)(n-2)$	$\frac{5}{2}(n-1)(3n-2)$
N_{fcc}	$\frac{10}{3}(n-1)(n-2)(n-3)$	$\frac{5}{6}n(n-1)(4n-5)$
N_{interior}	$(2n-1)[\frac{5}{3}n(n-1)+1]$	$\frac{10}{3}n^3-\frac{19}{3}n+4$
N	$(2n+1)[\frac{5}{3}n(n+1)+1]$	$\frac{10}{3}n^3+10n^2+\frac{11}{3}n+1$

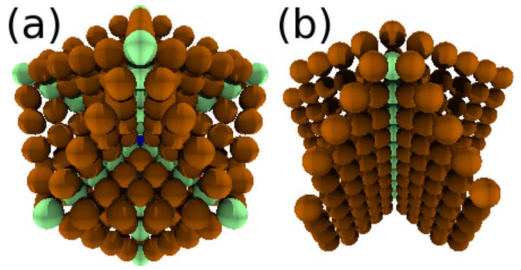

FIG. 6. (Color online) Position of ico (blue/black), dec (green/light gray), and hcp (orange/dark gray) atoms in the ground-state LJ cluster at size (a) $N=923$ (Mackay icosahedron) and (b) $N=1103$ (Marks decahedron), showing large-scale structural organization.

the C_{60} clusters (open symbols) computed using the Pacheco and Prates–Ramalho potential.[19] Most of the LJ clusters in this size range has a single icosahedron motif (not shown) at the core and no fcc-coordinated atoms. Their structure essentially follows that of the Mackay icosahedra series, with modifications close to the surface layer. Notable exceptions are found at $N=38$ (fcc) and $N=75-77$ (Marks decahedron), as seen in Fig. 7(a) where the fcc content takes a nonzero value.

The C_{60} clusters behave quite differently from the LJ clusters. The icosahedron core is present only at $N\leq 15$. About one third of the clusters in the size range of 31–100 are cubic (i.e., with only fcc and hcp motifs), whereas the rest contain some form of the decahedral structure. It has been suggested that, due to the narrow range of the molecular potential, C_{60} clusters prefer close-packed structures as compared to the LJ clusters.[19,20] This is in good agreement with the much higher percentage of fcc and hcp motifs in the composition profiles

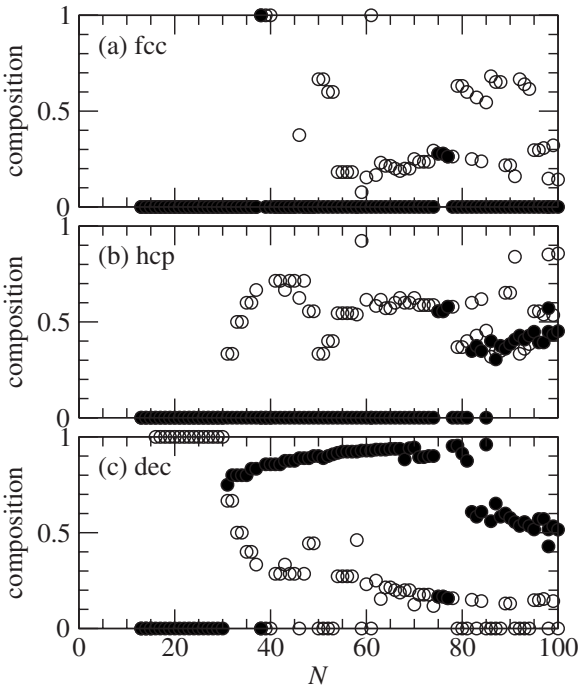

FIG. 7. Motif composition profiles for Lennard-Jones (solid symbols) and C_{60} (open symbols) clusters below $N=100$. (a) fcc, (b) hcp, and (c) dec.

as shown in Figs. 7(a) and 7(b). We have also examined the different series of the ground-state Morse clusters in the CCD that correspond to a broad range of softness of the pair potential.[21] Indeed, as the range of the interaction shortens, a change from the icosahedral to decagonal and cubic structures is observed.

The decahedral motif plays a key role in the large-scale structural organization due to its unique pentagonal symmetry axis. In both the Mackay icosahedra and Marks decahedra series, decahedra motifs stack together to form linear chains to propagate the (local) pentagonal symmetry all the way to the cluster surface. Two or more pentagonal axes can emanate from an icosahedral motif or an incomplete icosahedron at the surface. Chains of decahedra have also been observed in less ordered LJ clusters by Polak.[11,12] The network of decahedral motifs (plus their orientation), to a great degree, defines the overall structure of these low-energy atomic clusters.

IV. SUMMARY AND CONCLUSIONS

In summary, we have presented a general method to identify reoccurring local structural units in an atomic cluster without prior information. The structural units, taken here to be atoms on the first coordination shell, are represented by a set of multipole moments whose clustering properties form the basis for robust and efficient classification schemes. Applying the scheme to the ground state of the LJ and C_{60} clusters, we reconfirmed that the fcc, hcp, ico, and dec motifs provide a complete set of the 12-atom neighborhood for all interior atoms. For the LJ clusters, the motif compositions show a systematic dependence on cluster size, in agreement with the existing understanding on the structure evolution of these clusters. Large-scale structural organization is readily revealed when interior atoms are displayed according to their coordination type. Under this scheme, the level of complexity in structure representation is significantly reduced. This "microstructure" characterization can play an important role in the development of coarse-grained models that combine geometry and energetics to elucidate the equilibrium and kinetic properties of medium-sized atomic clusters at low temperatures.

The study of noisy atomic clusters allows one to relate the size and shape of the cloud surrounding each ideal shell structure in the shape space to the actual displacement of atoms in the physical space. Interestingly, the noise level at which the clouds for different coordination motifs overlap coincides well with the one given by the Lindemann criterion for crystal melting. This observation offers a potentially fruitful way to analyze melting in superheated solids[22] in terms of the local coordination patterns and their spatial distribution.

ACKNOWLEDGMENTS

We wish to thank X.-G. Shao for providing the LJ cluster coordinates in the size range of 1001–1610. This work was supported by the Research Grants Council of the HKSAR through Grant No. HKBU 2020/04P.

[1] G. Schmid, M. Bäumle, M. Geerkens, I. Heim, C. Osemann, and T. Sawitowski, Chem. Soc. Rev. **28**, 179 (1999).
[2] F. Baletto and R. Ferrando, Rev. Mod. Phys. **77**, 371 (2005).
[3] M. Walter, J. Akola, O. Lopez-Acevedo, P. D. Jadzinsky, G. Calero, C. J. Ackerson, R. L. Whetten, H. Grönbeck, and H. Häkkinen, Proc. Natl. Acad. Sci. U.S.A. **105**, 9157 (2008).
[4] D. J. Wales, *Energy Landscapes* (Cambridge University Press, Cambridge, 2003).
[5] T. P. Martin, Phys. Rep. **273**, 199 (1996).
[6] A. L. Mackay, Acta Crystallogr. **15**, 916 (1962).
[7] L. D. Marks, Philos. Mag. A **49**, 81 (1984).
[8] V. Kiryukhin, E. P. Bernard, V. V. Khmelenko, R. E. Boltnev, N. V. Krainyukova, and D. M. Lee, Phys. Rev. Lett. **98**, 195506 (2007).
[9] N. V. Krainyukova, Eur. Phys. J. D **43**, 45 (2007).
[10] B. W. van de Waal, G. Torchet, and M.-F. de Feraudy, Chem. Phys. Lett. **331**, 57 (2000).
[11] W. Polak and A. Patrykiejew, Phys. Rev. B **67**, 115402 (2003).
[12] W. Polak, Phys. Rev. E **77**, 031404 (2008).
[13] P. J. Steinhardt, D. R. Nelson, and M. Ronchetti, Phys. Rev. B **28**, 784 (1983).
[14] http://www-wales.ch.cam.ac.uk/CCD.html
[15] X. Shao, Y. Xiang, and W. Cai, J. Phys. Chem. A **109**, 5193 (2005).
[16] A. K. Jain, M. N. Murty, and P. J. Flynn, ACM Comput. Surv. **31**, 264 (1999).
[17] R. W. Cahn, Nature (London) **413**, 582 (2001).
[18] J. P. K. Doye and F. Calvo, J. Chem. Phys. **116**, 8307 (2002).
[19] J. P. K. Doye, D. J. Wales, W. Branz, and F. Calvo, Phys. Rev. B **64**, 235409 (2001).
[20] J. P. K. Doye and D. J. Wales, Chem. Phys. Lett. **247**, 339 (1995).
[21] J. P. K. Doye and D. J. Wales, J. Phys. B **29**, 4859 (1996).
[22] Z. H. Jin, P. Gumbsch, K. Lu, and E. Ma, Phys. Rev. Lett. **87**, 055703 (2001).